Supplemental materials

Figure S1

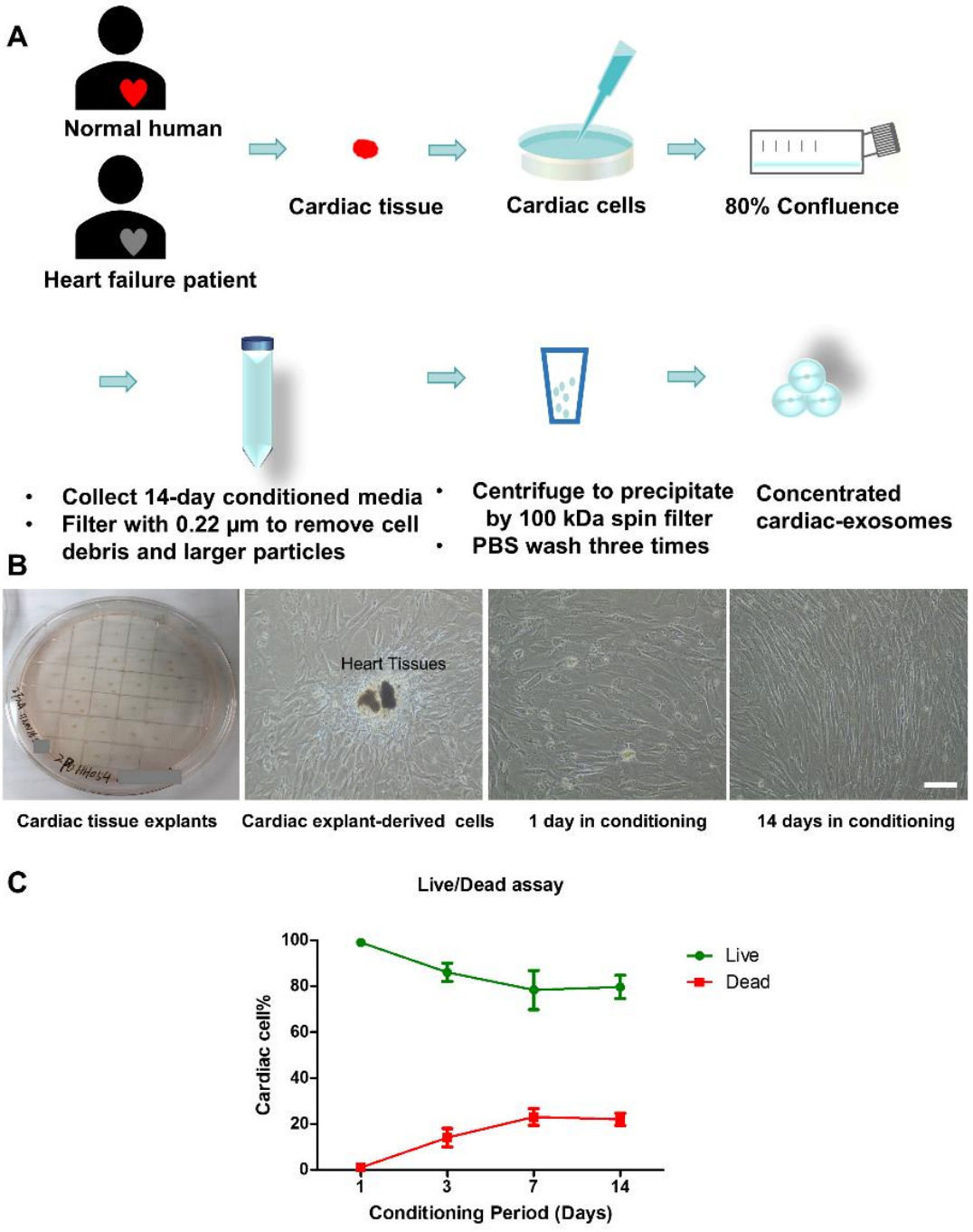

Figure S1. Isolation of exosomes from cardiac explant-derived cells. (A) Derivation of cardiac cells and exosomes. (B) Representative images of explant culture, outgrowth cells from explant tissues, and the cardiac cells before and after 14-day conditioning. Scale bar: 100μm. (C) Live/Dead assay showing cell viability during the conditioning period (n=3).

Figure S2

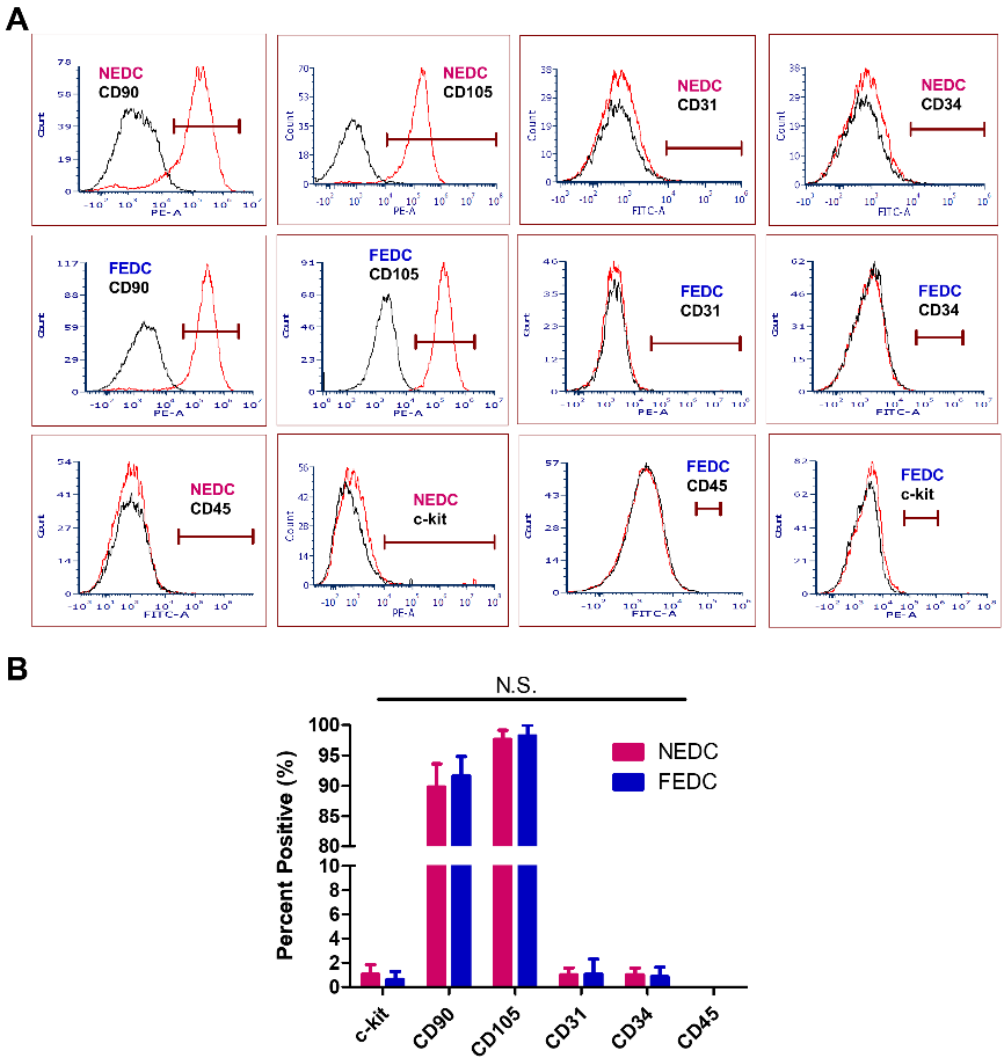

Figure S2. Phenotypic analysis of explant-derived cardiac cells. (A) Representative flow cytometry histogram of cardiac cells derived from heart failure patients (FEDC) or healthy heart donors (NEDC). The expressions of CD90, CD105, CD31, CD34, CD45, and c-kit are examined. Black lines in the histograms are the unstained or isotype controls. Red lines show the particular markers. (B) Quantitative analyses of CD90, CD105, CD31, CD34, CD45, and c-kit expressions (n=3-4). N.S., no significance. Two-tailed t-test. All values are mean ± S.D.

Figure S3

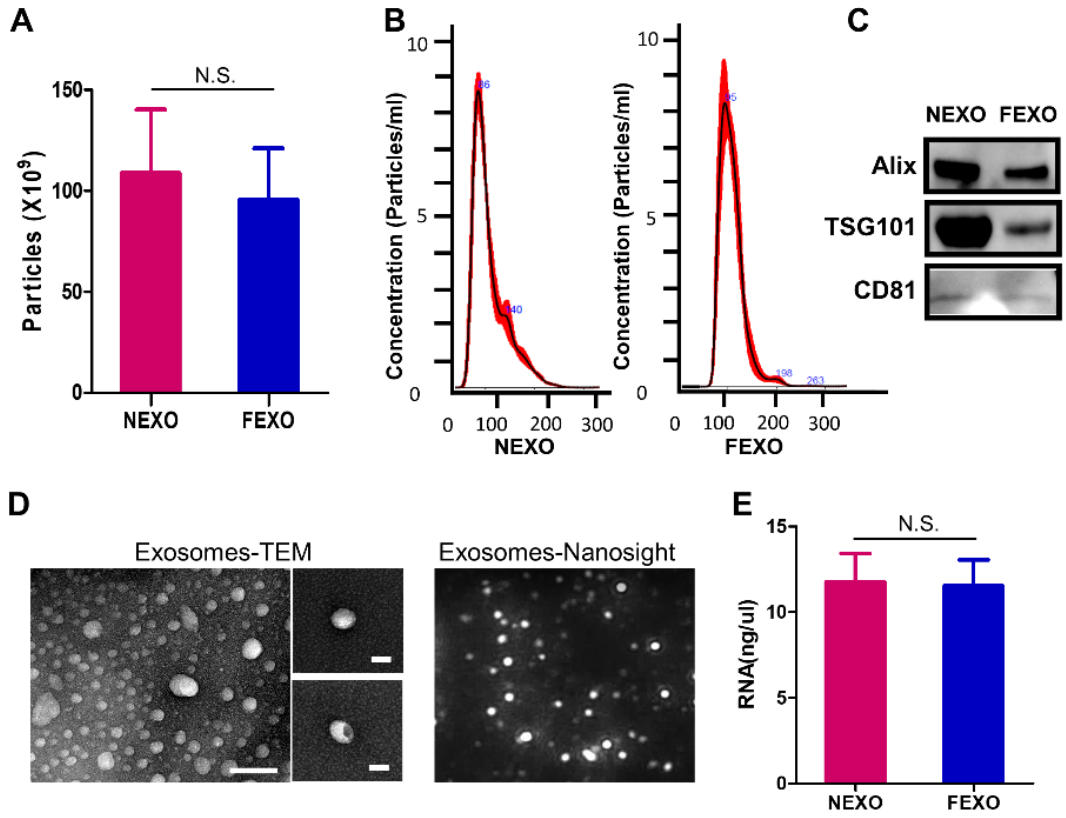

Figure S3. Characterization of exosomes from normal and failing hearts. (A) Exosome quantitation using NanoSight particle tracking images (n = 3 biological replicates, 5 technical replicates for each biological replicate). (B) Size distribution of NEXO and FEXO by NanoSight showing that the exosomes are within the expected size range. (C) NEXO and FEXO express exosomal markers Alix, TSG 101, and CD81 as revealed by western blot analysis. (D) Transmission electron microscopy (TEM) and NanoSight showing exosome morphology and motion. Scale bar: 100 μm. (E) Total RNA content measured in NEXO and FEXO by Nanodrop (n = 3 biological replicates). N.S., no significance. Two-tailed t-test. All values are mean ± S.D. FEXO, exosomes derived from the cardiac cells of heart failure patients. NEXO, exosomes derived from the cardiac cells of normal heart donors.

Figure S4

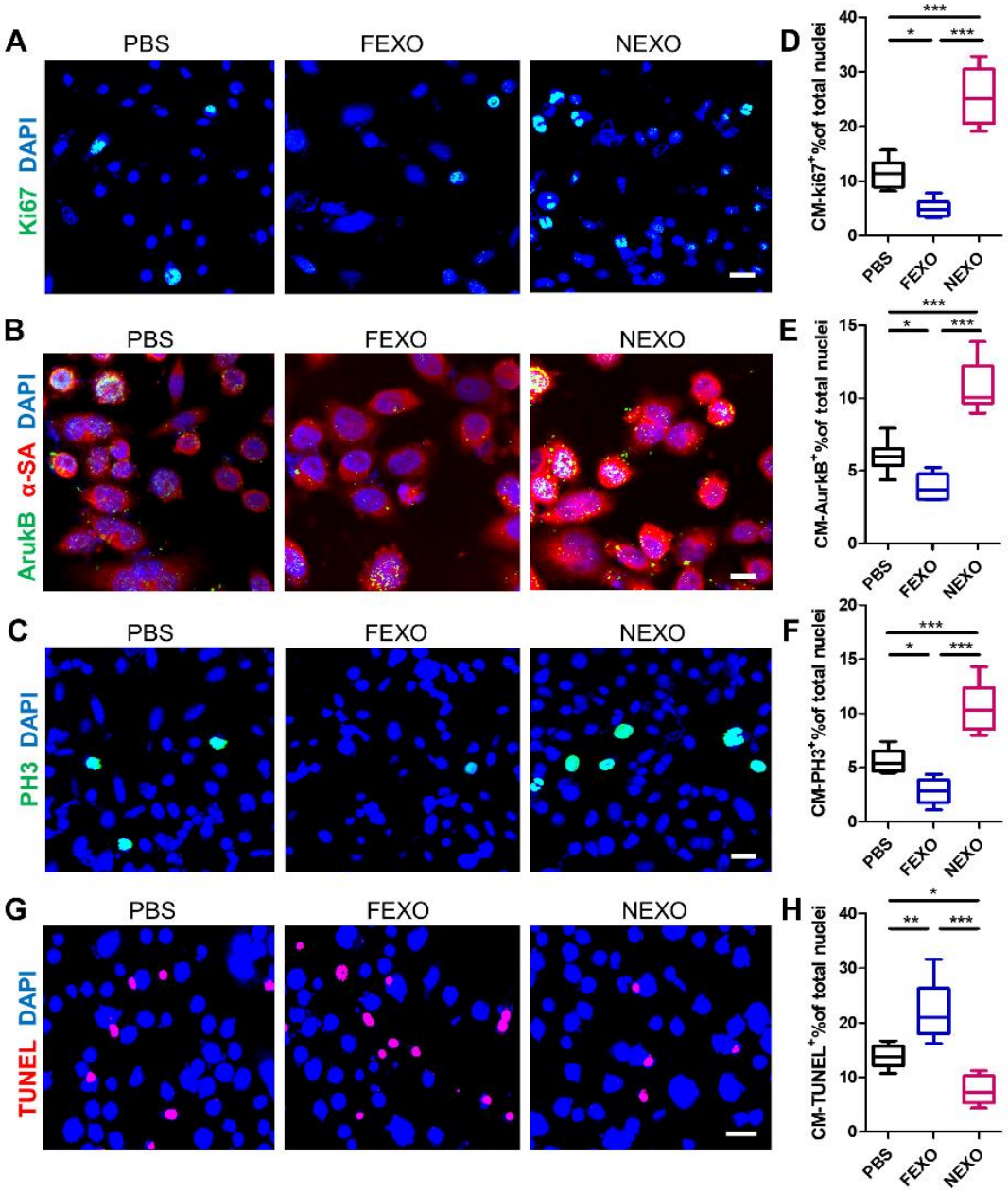

Figure S4. Effects of NEXO or FEXO treatment on cardiomyocytes in vitro. (A-C) Representative fluorescent micrographs showing adult human cardiomyocyte proliferation in response to NEXO, FEXO, or PBS treatment. Scale bar: 20 μm. (D-F) Quantitation of cardiomyocyte proliferation, as detected by three proliferation markers: AURKB, Ki67, and PH3 (n=6). (G) Representative fluorescent micrographs showing adult human cardiomyocyte apoptosis in response to NEXO, FEXO, or PBS treatment. Scale bar: 20 μm. (H) Quantitation of apoptotic cardiomyocytes detected by TUNEL (n=6). *, p<0.05. **, p<0.01. ***, p<0.001. One-way ANOVA with Bonferroni post correction. All values are mean ± S.D. FEXO, exosomes derived from the cardiac cells of heart failure patients. NEXO, exosomes derived from the cardiac cells of normal heart donors.

Figure S5

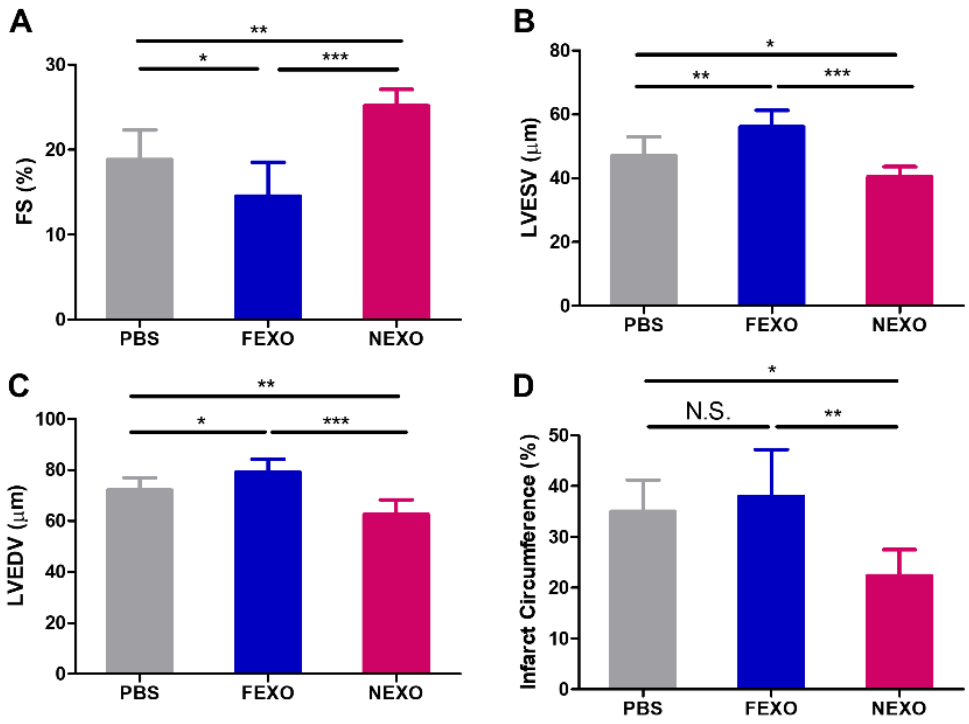

Figure S5. Effects of NEXO or FEXO therapy on cardiac function and morphometry. (A-C) Echocardiographic measurements of fractional shortening (FS) (A), left ventricular end systolic volume (B), and left ventricular end diastolic volume (C) of MI hearts treated with NEXO, FEXO, or PBS. (D) Quantitative analysis of circumference of scar tissue. n=6 animals per group. *, $p<0.05$. **, $p<0.01$. ***, $p<0.001$. N.S., no significance. One-way ANOVA with Bonferroni post correction. All values are mean ± S.D. FEXO, exosomes derived from the cardiac cells of heart failure patients. NEXO, exosomes derived from the cardiac cells of normal heart donors.

Figure S6

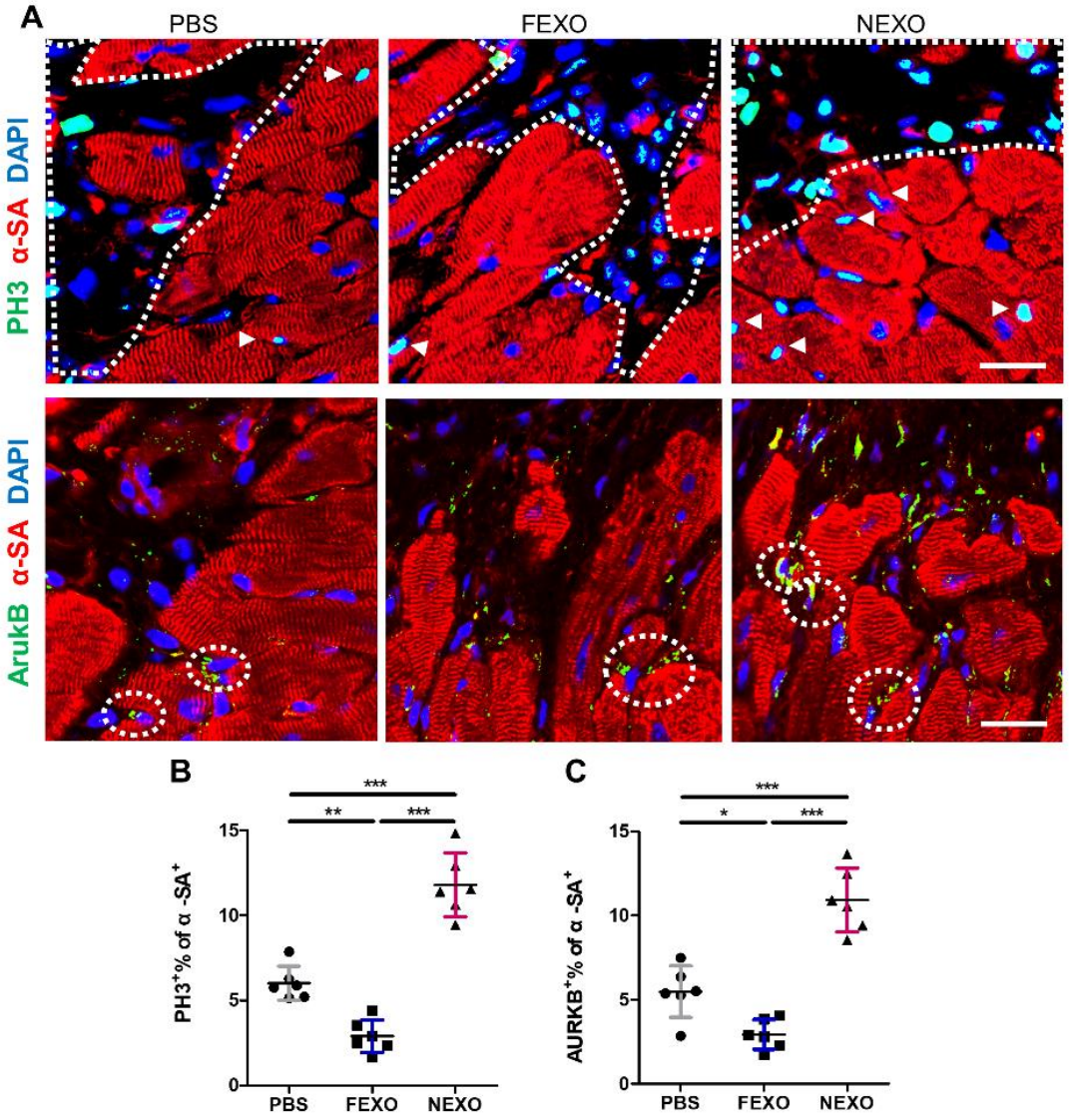

Figure S6. Effects of NEXO or FEXO treatment on cardiomyocyte proliferation in vivo. (A) Representative images of post-MI heart sections stained with mitosis marker PH3 or cytokinesis marker ARUKB. Scale bar: 20μm. (B-C) Quantitation of proliferated cardiomyocytes (n=6). *, p<0.05. **, p<0.01. ***, p<0.001. One-way ANOVA with Bonferroni post correction. All values are mean ± S.D. FEXO, exosomes derived from the cardiac cells of heart failure patients. NEXO, exosomes derived from the cardiac cells of normal heart donors.

Figure S7

A

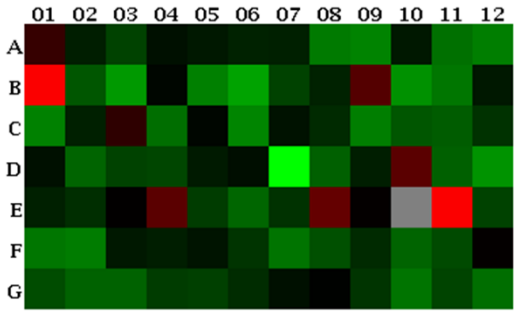

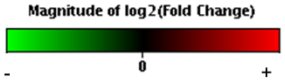

B

A01 hsa-let-7a-5p	A02 hsa-let-7b-6p	A03 hsa-let-7c-6p	A04 hsa-let-7d-7p	A05 hsa-let-7e-7p	A06 hsa-let-7f-8p	A07 hsa-miR-1-3p	A08 hsa-miR-100-5p	A09 hsa-miR-103a-3p	A10 hsa-miR-107	A11 hsa-miR-10b-5p	A12 hsa-miR-122-5p
B01 hsa-miR-124-3p	B02 hsa-miR-125a-5p	B03 hsa-miR-125b-5p	B04 hsa-miR-126-3p	B05 hsa-miR-130a-3p	B06 hsa-miR-133a-3p	B07 hsa-miR-133b	B08 hsa-miR-140-5p	B09 hsa-miR-142-3p	B10 hsa-miR-143-3p	B11 hsa-miR-144-3p	B12 hsa-miR-145-5p
C01 hsa-miR-146-5p	C02 hsa-miR-149-5p	C03 hsa-miR-150-5p	C04 hsa-miR-155-5p	C05 hsa-miR-15b-5p	C06 hsa-miR-16-5p	C07 hsa-miR-17-5p	C08 hsa-miR-181a-5p	C09 hsa-miR-181b-5p	C10 hsa-miR-182-5p	C11 hsa-miR-183-5p	C12 hsa-miR-185-5p
D01 hsa-miR-18b-5p	D02 hsa-miR-195-5p	D03 hsa-miR-199-5p	D04 hsa-miR-206	D05 hsa-miR-208a-3p	D06 hsa-miR-208b-3p	D07 hsa-miR-21-5p	D08 hsa-miR-26b-4p	D09 hsa-miR-214-3p	D10 hsa-miR-22-3p	D11 hsa-miR-221-3p	D12 hsa-miR-222-3p
E01 hsa-miR-223-3p	E02 hsa-miR-224-5p	E03 hsa-miR-23a-3p	E04 hsa-miR-23b-3p	E05 hsa-miR-24-3p	E06 hsa-miR-25-3p	E07 hsa-miR-26a-5p	E08 hsa-miR-210-3p	E09 hsa-miR-27a-3p	E10 hsa-miR-27b-3p	E11 hsa-miR-29a-3p	E12 hsa-miR-29b-3p
F01 hsa-miR-29c-3p	F02 hsa-miR-302a-3p	F03 hsa-miR-302b-3p	F04 hsa-miR-30a-5p	F05 hsa-miR-30c-5p	F06 hsa-miR-30d-5p	F07 hsa-miR-30a-5p	F08 hsa-miR-31-5p	F09 hsa-miR-320a	F10 hsa-miR-328-3p	F11 hsa-miR-342-3p	F12 hsa-miR-365a-3p
G01 hsa-miR-378a-3p	G02 hsa-miR-423-3p	G03 hsa-miR-424-5p	G04 hsa-miR-451a	G05 hsa-miR-3486-5p	G06 hsa-miR-494-3p	G07 hsa-miR-499a-5p	G08 hsa-miR-7-5p	G09 hsa-miR-92a-3p	G10 hsa-miR-93-5p	G11 hsa-miR-98-5p	G12 hsa-miR-99a-5p

C

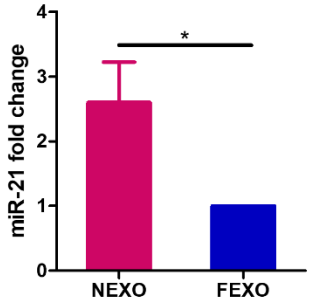

Figure S7. Heat map of microRNA PCR array identifies miR-21-5p as the most differentially expressed microRNA between NEXO and FEXO. (A-B) Heat map showing miRs fold changes between NEXO and FEXO. (C) Infarcted mouse hearts treated with NEXO have elevated levels of miR-21 compared to FEXO-treated hearts. n = 3 animals per group. *, $p<0.05$. Two-tailed t-test. All values are mean ± S.D. FEXO, exosomes derived from the cardiac cells of heart failure patients. NEXO, exosomes derived from the cardiac cells of normal heart donors.

Figure S8

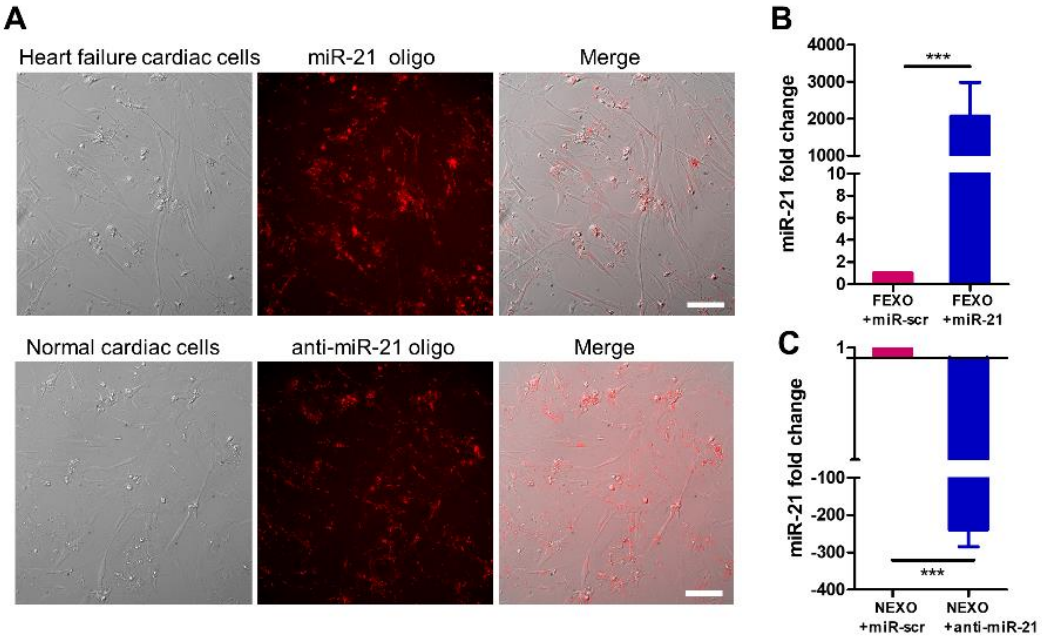

Figure S8. Direct manipulation of miR-21 in NEXO and FEXO. (A) Transfection of cardiac cells from heart failure patients/healthy heart donors with miR-21/ anti-miR-21 oligo or scrambled miR oligo (as a negative control). Scale bar: 100μm. (B, C) Transfection efficiency of mi-R21/anti-miR-21 oligo was determined by qRT-PCR. n=3 biological replicates. ***, $p<0.001$. Two-tailed t-test. All values are mean ± S.D. FEXO+miR-scr, exosomes derived from the cardiac cells of heart failure patients transfected with scrambled miR oligo. FEXO+miR-21, exosomes derived from the cardiac cells of heart failure patients transfected with miR-21-5p oligo. NEXO+miR-scr, exosomes derived from the cardiac cells of the normal hearts transfected with scrambled miR oligo. NEXO+anti-miR-21, exosomes derived from the cardiac cells of the normal hearts transfected with anti-miR-21-5p oligo.

Figure S9

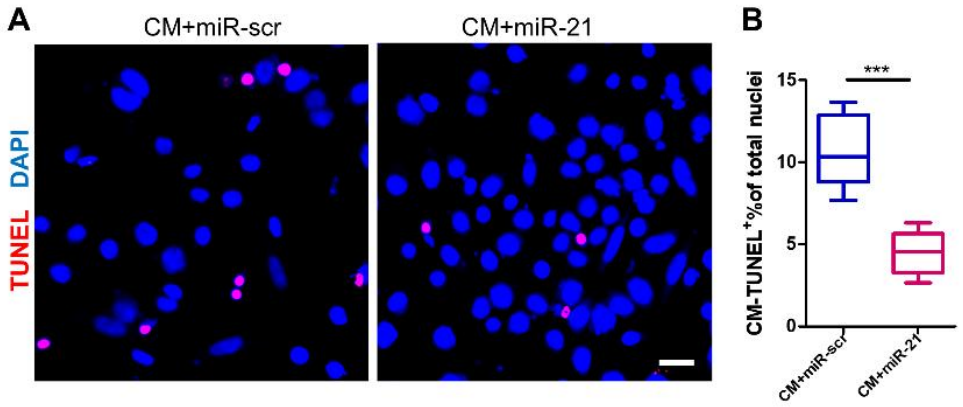

Figure S9. Effects of miR-21 on adult human cardiomyocytes in vitro. Adult human cardiomyocytes were transfected with miR-21-5p mimic or scrambled control. (A) Representative images of transfected human cardiomyocytes stained with TUNEL. Scale bar: 20μm. (B) Quantitation of cardiomyocyte apoptosis (n=6). ***, p<0.001. Two-tailed t-test. All values are mean ± S.D. CM+miR-scr, human cardiomyocytes transfected with scrambled miR. CM+miR-21, human cardiomyocytes transfected with miR-21-5p mimic.

Figure S10

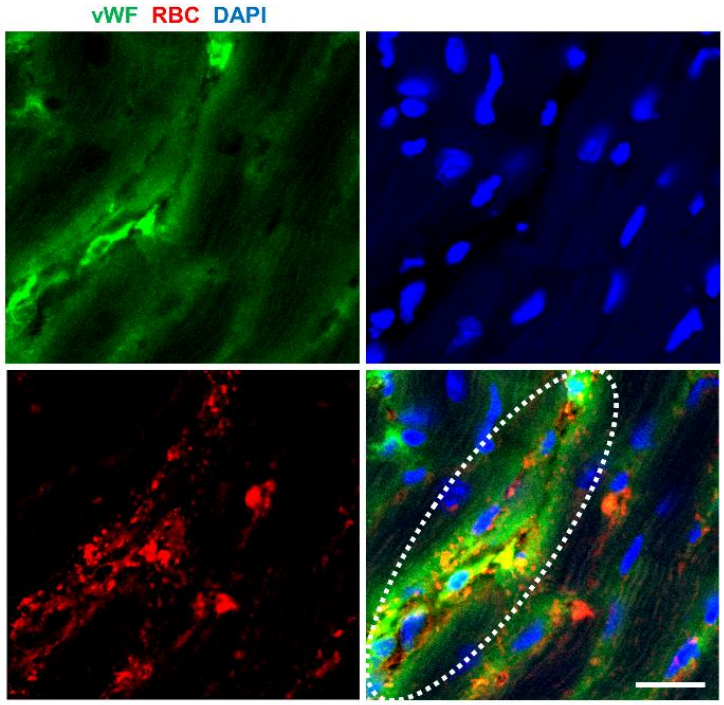

Figure S10. Pro-angiogenic effects of miR-21 on post-MI heart. Functional vessels were confirmed by co-staining of the endothelial cell marker von Willebrand factor (vWF) and the red blood cell (RBC) marker. RBCs were detected in the blood vessels in the MI border zone of the heart treated with miR-21-over-expressed FEXO. FEXO, exosomes derived from the cardiac cells of heart failure patients. Scale bar: 20 μm.

Figure S11

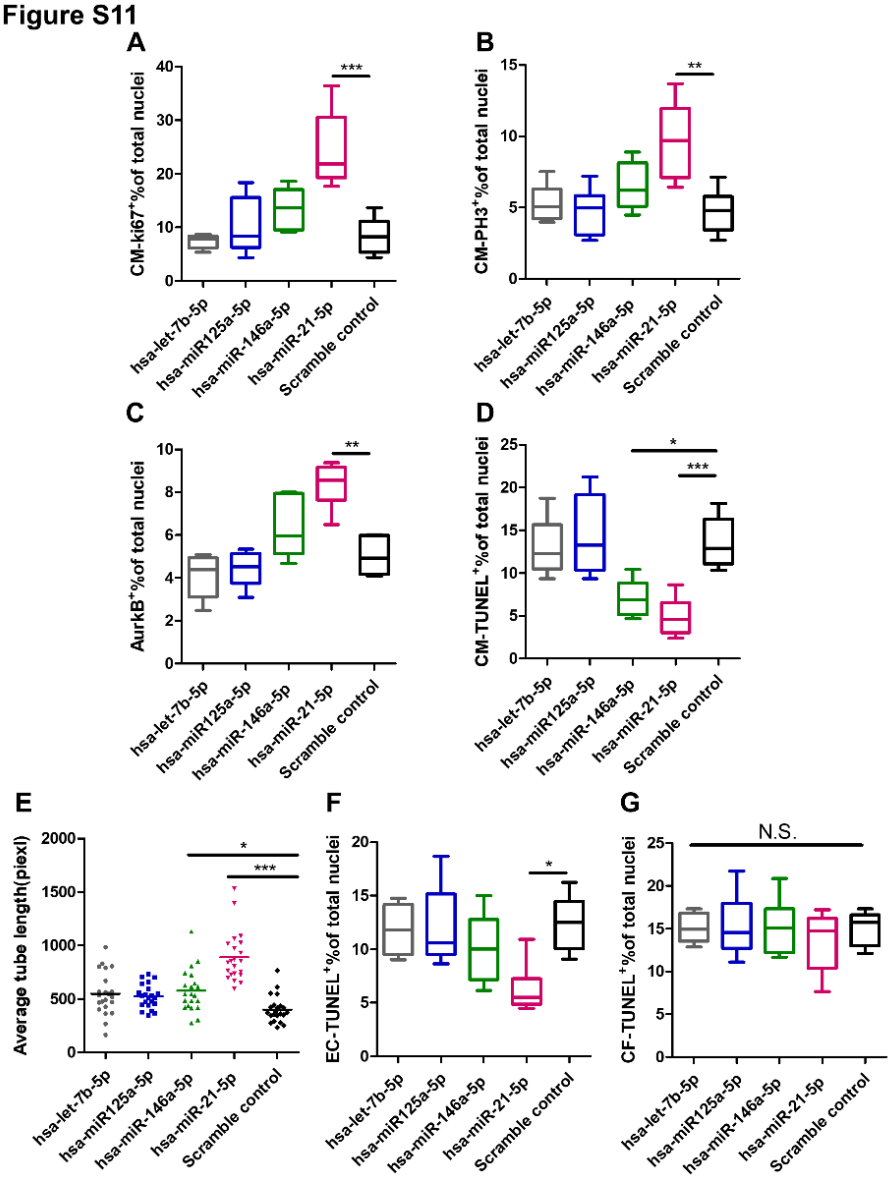

Figure S11. Effects of various microRNA treatments on cardiomyocytes, endothelial cells, and cardiac fibroblasts in vitro. Human cardiomyocytes (CM), human cardiac fibroblasts (CF), and human umbilical vein endothelial cells (HUVECs) were treated with let-7b-5p, miR-125a-5p, miR-146a-5p, miR-21-5p mimics or scrambled control, followed by immunocytochemistry staining of proliferation or apoptotic markers. (A-C) Cardiomyocyte proliferation in response to let-7b-5p, miR-125a-5p, miR-146a-5p or miR-21-5p, as calculated by three proliferation markers: Ki67, phospho-histone H3 (PH3, mitosis marker), and aurora kinase B (AURKB, cytokinesis marker) (n=6). (D) Apoptotic cardiomyocytes transfected with indicated miRs (n=6). (E) Measurement of tube length in HUVECs in the transfection of indicated miRs (n=22). (F-G) Quantitation of apoptosis of HUVECs (F) and cardiac fibroblasts (G) after transfection with indicated miRs (n=6). *, $p<0.05$. **, $p<0.01$. ***, $p<0.001$. N.S., no significance. One-way ANOVA with Bonferroni post correction. All values are mean ± S.D.

Figure S12

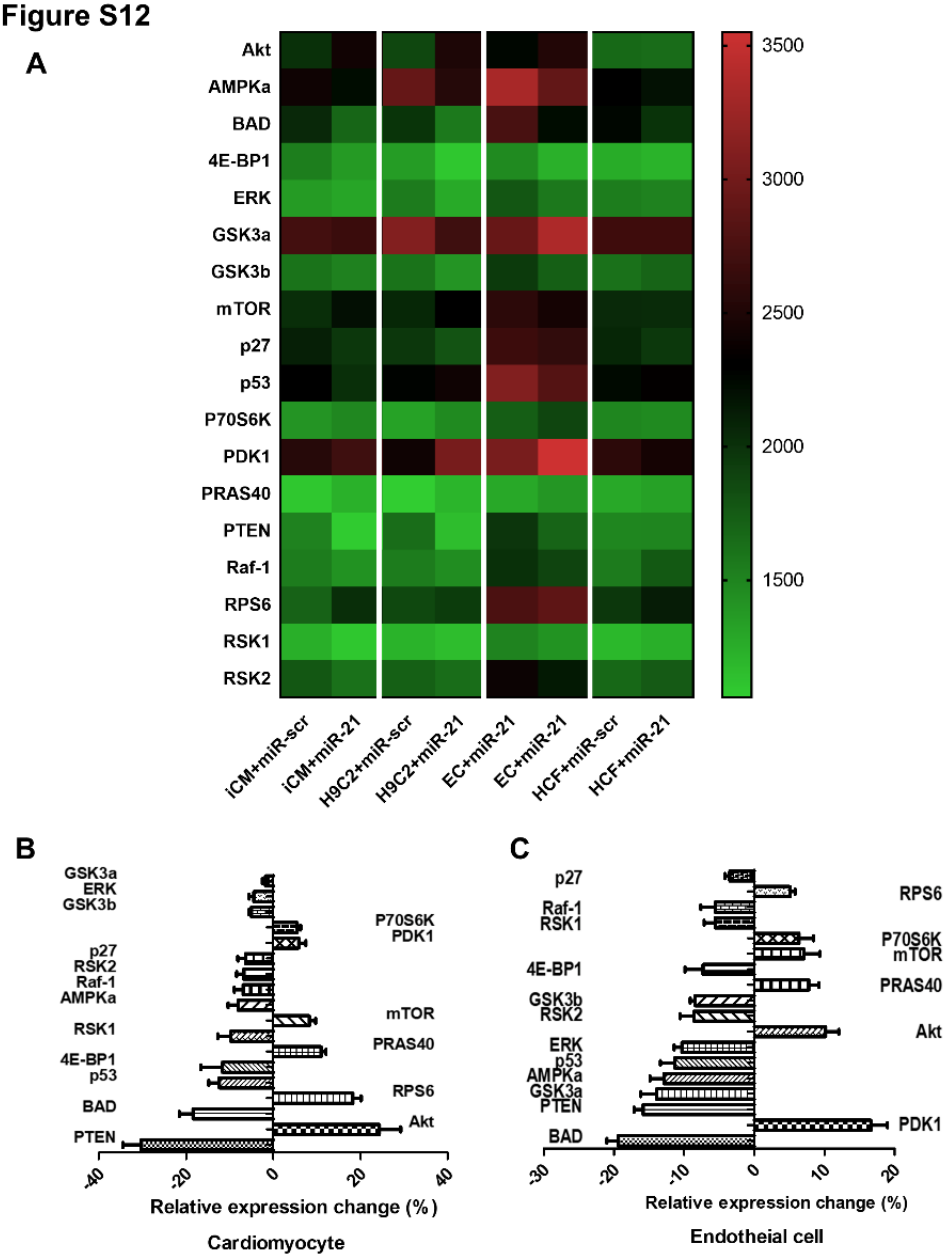

Figure S12. Signaling pathway phosphorylation array identifies PTEN/Akt as the miR-21-regulate genes in cardiomyocytes and endothelial cells. Three major cell types in the heart (cardiomyocytes (CM), endothelial cells (EC), and cardiac fibroblasts (CF)) were treated with miR-21 mimic or scrambled control, followed by the examination of 18 phosphorylated proteins with a signaling pathway phosphorylation array. (A) Heat map showing expression level changes between cells transfected with miR-21 mimic or scrambled control. (B) Quantitation of expression changes in miR-21-upregulated cells relative to scrambled control. (n = 2 biological replicates, 2 technical replicates for each biological replicate). All values are mean ± S.D. Cardiomyocytes (using both human induced pluripotent stem cell-derived cardiomyocytes (iCM) and H9C2 cells), cardiac fibroblasts (using human cardiac fibroblasts, HCF), and endothelial cells (using human umbilical vein endothelial cells, HUVECs).